Chapter 7: Fundamentals on the Topological Derivative concept and its classical applications

Fundamentals on the Topological Derivative concept and its classical applications

Fernando Soares de Carvalho[1], Carla Tatiana Mota Anflor[2*],
Ariosto Bretanha Jorge[2], Adrián Pablo Cisilino[3], Rogério José Marczak[4].

[1]Math, Federal University of Tocantins, Arraias, Tocantins, Brazil, e-mail: fscarvalho@uft.edu.br
[2*]Post-Graduate Program - Integrity of Engineering Materials, University of Brasilia, Brazil. E-mail:
anflor@unb.br, ariosto.b.jorge@gmail.com
[3]Department of Mechanical Engineering INTEMA, Universidad Nacional de Mar del Plata, Argentina, e-mail:
cisilino@fi.mdp.edu.ar
[4] Department of Mechanical Engineering, Federal University of Rio Grande do Sul, Brazil, e-mail:
rato@mecanica.ufrgs.br

*Corresponding author: anflor@unb.br

Abstract

The concept of the topological derivative has been derived for several engineering problems during the last years. In this chapter, the fundamentals and the resulting closed formulae of topological derivative for some of the most classical problems are addressed. A brief review of the mathematical statements used in the topological derivative concept is given. The programming strategies regarding implementing the main routine for the topology optimization are pointed out. Some numerical examples concerning classical applications are introduced to demonstrate the application of the topological derivative concept for topology problems.

1   Introduction

Topological sensitivity analysis was presented as a technique that allows obtaining simultaneously the optimal shape and topology, being proposed originally by (Schumacher [1996], Sokołowski and Żochowski [1997], Sokolowski and Zochowski [1999], Garreau et al. [1998], Garreau et al. [2001]). This sensitivity calculation results in a scalar function called a topological derivative (D_T). The D_T provides for each point in the domain the sensitivity of the cost function when creating a small hole at that point.Garreau et al. [1998]), proposed the truncated domain method to calculate the topological derivative. The proposed method was based on some simplifying assumptions, the most severe of which consisted in the fact that the cost function should not explicitly depend on the domain. The works of Sokolowski and Zochowski [1999] and Céa et al. [2000] presented the calculation of D_T, via shape sensitivity analysis, particularized only for cases where the homogeneous Neumann boundary condition was prescribed in the holes. The other boundary conditions, such as non-homogeneous Neumann, Dirichlet and Robin do not validate their applicability in this calculation hypothesis. Novotny et al. [2003]

precisely establish the concepts of derived topology and shape change sensitivity analysis for isotropic materials. This last methodology does not present any limitation regarding the cost function or the type of boundary condition prescribed in the holes. Since then several classes of engineering and physics problems have been solved by employing the D_T concept, for instance, topology optimization ([Amstutz and Novotny [2010], Novotny et al. [2007]]), inverse analysis ([Carpio and Rapún [2008], Rocha and Novotny [2017]]), and image processing ([Hintermüller and Laurain [2009], Larrabide et al. [2008]]). The D_T was also computed using the Boundary Element Method (BEM) for topology optimization of potential (Anflor [2007],Anflor and Marczak [2009], Anflor et al. [2014]) and elasticity (Marczak [2008], Bertsch et al. [2008], Anflor et al. [2018]) problems as an alternative to the Finite Element Method (FEM) employed as the standard numerical solver. All advantages provided by BEM as a boundary method were taken into account showing the efficiency of the developed methodology for optimization problems. Another class of problem of great interest concerns the damage identification in structures. The identification of flaws by the inverse problem was generally solved by heuristic algorithms where the information about sensitivity or gradient of the cost functional with respect to design parameters are not needed. Despite the success of the use of these algorithms, the computational cost was still high because a large number of direct problems has to be evaluated and solved. The computational time can be drastically reduced by using the cost functional topological sensitivity instead of the full functional (Comino et al. [2008]). In addition, the use of topological sensitivity coupled to heuristic algorithms increases the accuracy for estimating the location and size of defects. The concept of D_T becomes naturally attractive and suitable for problems concerning damage detection, once the D_T measures the sensitivity of a functional shape with respect to an infinitesimal singular domain perturbation. The perturbation may be represented as damages in the structure in the shape of holes, inclusions, sources terms, or even cracks. The topological sensitivity analysis was carried out for the Laplace equation to identify arbitrary shaped cracks in two-dimensional domains (Amstutz et al. [2005]). A method based on the multi-frequency D_T was developed as an alternative to standard guided-waves-based Structural Health Monitoring (SHM) methods and used for locating the presence of flaws in thin plates (Martinez Dominguez et al. [2018]). The damage identification based on the D_T method was addressed in (da Silva and Novotny [2022]) for problems governed by the elastodynamic Kirchhoff and Reissner-Mindlin plate bending models in the frequency domain. According to this brief review, the reader can have an idea about the wide range of the use of D_T in physical phenomena modeled by partial differential equations. In the remainder of this chapter, the fundamentals on D_T for classical problems of topology optimization are introduced, and some numerical examples are presented, showing the efficiency and applicability of this concept for generating optimal geometries.

2   Topological derivative considering the insertions as voids

The theory behind the D_T is the evaluation of a given cost function when a small hole of radius is open inside the domain, as shown in 1.
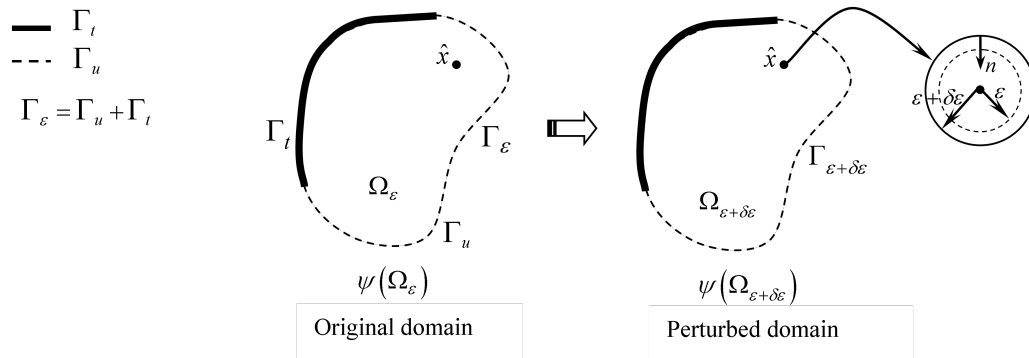
Figure 1: The new concept of the topological derivative and the boundary conditions

In this sense, the concept of D_T consists of determining the sensitivity of a given function cost (ψ) when this small hole is increased or decreased. The local value of the D_T at a point $\hat{x}$ inside the domain for this case is given by eq. 1:

$$D_T(\hat{x}) = \lim_{\varepsilon \to \infty} \frac{\psi(\omega_\varepsilon) - \psi(\omega)}{f(\varepsilon)}, \tag{1}$$

where $\psi(\omega)$ and $\psi(\omega_\epsilon)$ are the cost function evaluated for the original domain and the perturbed domain, respectively, and (f) is a problem-dependent regularizing function. It is important to highlight that it is not possible to establish an isomorphism between domains with different topologies using eq.1. A new concept regarding the D_T was introduced by Novotny et al. (2003) that allowed the non-isomorphism between the original and the modified domains to be overcome. The mathematical idea was based on the creation of a hole that can be accomplished by a single perturbation to an existing hole with radius tending to zero. This allows the restatement of the such a way that it is possible to establish a mapping between them, as presented in eq.2:

$$D_T(\hat{x}) = \lim_{\varepsilon \to \infty} \frac{\psi(\omega_{\varepsilon+\delta\epsilon}) - \psi(\omega_\varepsilon)}{f(\Omega_{\varepsilon+\delta_\varepsilon}) - f(\Omega_\varepsilon)}, \tag{2}$$

where δ is a small perturbation of the hole's radius. It's worth mention that eq.2 is a general definition for D_T. This section introduces the D_T particularized for some of the classical engineering problems.

2.1   Potential problems

In the case of isotropic linear heat transfer problems, the direct problem is stated as: Find u_ε, such that

$$
\begin{cases}
-k\nabla u_\varepsilon &= b & \text{in} & \Omega\,, \\
u_\varepsilon &= u & \text{on} & \Gamma_D, \\
k\partial_n u &= q & \text{on} & \Gamma_N, \\
k\partial_n u_\varepsilon &= h_\varepsilon(u_\varepsilon - u_\infty) & \text{on} & \Gamma_R, \\
h(\alpha, \beta, \gamma) &= 0 & \text{on} & \Gamma_\varepsilon,
\end{cases}
\tag{3}
$$

Γ_ϵ stands for the holes boundary and

$$
h(\alpha, \beta, \gamma) = \alpha(u_\varepsilon - \bar{u}^\varepsilon) + \beta(k\frac{\partial u_\varepsilon}{\partial n} + \bar{q}^\varepsilon) + \gamma(k\frac{\partial u_\varepsilon}{\partial n} + h_c(u - \bar{u}_\varepsilon)),
\tag{4}
$$

is a function which takes into account the type of boundary condition on the perimeter of holes to be created. In eq. 4, u_ϵ and $\frac{du_\varepsilon}{dn} = q_\epsilon$ are the temperature and the flux on the hole boundary, while u_{inf}^ϵ and h_c^ϵ are the holeâs internal convection parameters, respectively. Suitable choices of α, β and γ define the type of boundary condition on the hole. One may impose $\alpha = 1$ and $\beta = \gamma = 0$ in eq. 4 if the Dirichlet b.c. is applied to the holes that are being opening during the iterative process. Using asymptotic expansions to include the effects of a hole inserted in Ω it is possible derive analytic expressions for $\Psi(\Omega_\varepsilon$ and $\Psi(\Omega_{\varepsilon+\delta\varepsilon})$, which are used to generate the final expressions for eq.2.

A general form for the cost function can be written as the total potential energy function,

$$
\Psi(\Omega_\tau) = \frac{1}{2}\int_{\Omega_\tau} \phi_{\Omega_\tau}(u_\tau)d\Omega_\tau + \int_{\Gamma_\tau} \phi_{\Gamma_\tau}(u_\tau)d\tau,
\tag{5}
$$

where τ is a parameter associate to the shape change velocity, i.e., $x_\tau(x) = x + \tau v(x)$. The sensitivity of the cost function with respect to τ can be derived from the *Gâteaux derivative* as,

$$
\frac{d}{d\tau}\Psi(\Omega_\tau)_{\tau=0} = \lim_{\tau\to 0} \frac{\Psi(\Omega_\tau - \Omega_{\tau=0})}{\tau} h(\alpha, \beta, \gamma) = 0,
\tag{6}
$$

In this case the problem can be re-stated as,

Evaluate: $\frac{d}{d_\tau}\Psi(\Omega_\tau) = 0$

Subject to,

$$
a_\tau(u_\tau, n_\tau) = l_\tau(n_\tau),\ \forall\ n_\tau \in \beta_\tau \text{ and } \forall\ \tau \geq 0,
\tag{7}
$$

where a is a continuous, coercive bilinear form, l_τ is a continuous linear functional and β_τ is the space of the admissible perturbation functions for the perturbed domain $\Omega\tau$. Using the total potential energy as a cost function ($\Psi_\tau(u_\tau) := \frac{1}{2}a_\tau(u_\tau, u_\tau) - l_\tau(u(\tau))$), the a_τ and l_τ functional are written as:

$$a_\varepsilon(u_\varepsilon, n_\varepsilon) := \int_{\Omega_\varepsilon} k\nabla u_\varepsilon \cdot \nabla \eta_\varepsilon \, d\Omega + \int_{\Gamma_\varepsilon} h_c u_\varepsilon \eta_\varepsilon \, d\Gamma + \int_{\partial \Lambda \varepsilon} h_c^\varepsilon u_\varepsilon \eta_\varepsilon \, d\partial\Lambda \qquad (8)$$

$$l_\varepsilon(n_\varepsilon) := \int_{\Omega_\varepsilon} b n_\varepsilon d\Omega - \int_\Gamma \overline{q}\eta_\varepsilon d\Gamma - \int_{\Gamma_c} h_c u_\infty \eta_\varepsilon d\Gamma + \int_{\partial \Lambda_\varepsilon \overline{q}_\varepsilon} \eta_\varepsilon d\partial\Lambda + \gamma \int_{\partial\Lambda_\varepsilon} h_c^\varepsilon u_\infty \eta_\varepsilon d\partial\Lambda$$
$$(9)$$

Equation 7 can be derived and the D_T particularized according to the boundary condition prescribed on the holes.

Neumann Boundary condition

When considering Neumann boundary condition eq.4 is set as $(\alpha = 0, \beta = 1, \gamma = 0)$ and the D_T is obtained by taking the limit as,

$$D_T(\hat{x}) = -\lim_{\varepsilon \to 0} \frac{1}{2f'(\varepsilon)} \int_{\partial\Omega\varepsilon} [k(\frac{\partial u_\varepsilon}{\partial t}) - k(\frac{\partial u_\varepsilon}{\partial n}) - 2bu_\varepsilon - \frac{2}{\varepsilon}\overline{q}_\varepsilon u_\varepsilon] \, d\Omega\varepsilon, \qquad (10)$$

where the variables t and n stand for the tangencial and normal directions, respectively.

In case of Neumann boundary conditions both cases can be considered, the homogeneous and non-homogeneous as introduced by eqs.11 and 12 , respectively

$$\overline{q}_\varepsilon = \frac{\partial u_\varepsilon}{\partial n}|_{\partial\Omega_\varepsilon} = 0 \text{ with } f'(\varepsilon) = -\pi\varepsilon^2, \qquad (11)$$

$$\overline{q}_\varepsilon = \frac{\partial u_\varepsilon}{\partial n}|_{\partial\Omega_\varepsilon} \neq 0 \text{ with } f'(\varepsilon) = -2\pi\varepsilon^2. \qquad (12)$$

Dirichlet Boundary Condition

For this case eq.5 can be particularized by setting the variables as $(\alpha = 1, \beta = 0, \gamma = 0)$ and the D_T is obtained by taking the limit as,

$$D_T(\hat{x}) = -\lim_{\varepsilon \to 0} \frac{1}{2f'(\varepsilon)} \int_{\partial\Omega\varepsilon} [k(\frac{\partial u_\varepsilon}{\partial t}) - k(\frac{\partial u_\varepsilon}{\partial n}) - 2bu_\varepsilon] \, d\Omega\varepsilon, \qquad (13)$$

being the conditions $u_\varepsilon = \overline{u_\varepsilon}$ and $\frac{\partial u_\varepsilon}{\partial t} \neq 0$, which are employed along with $f'(\varepsilon) = -\frac{2\pi}{\varepsilon \ln(\varepsilon)^2}$.

Robin Boundary Condition

In this case one has $(\alpha = 0, \beta = 0, \gamma = 1)$ and the D_T is obtained taking the limit as,

$$D_T(\hat{x}) = -\lim_{\varepsilon \to 0} \frac{1}{2f'(\varepsilon)} \int_{\partial\Omega\varepsilon} [k(\frac{\partial u_\varepsilon}{\partial t}) - k(\frac{\partial u_\varepsilon}{\partial n}) - 2bu_\varepsilon - \frac{2}{\varepsilon}h_c^\varepsilon(u_\varepsilon - 2u_{\varepsilon\infty})]d\Omega\varepsilon \qquad (14)$$

being the regularization function as $f'(\varepsilon) = -2\pi\varepsilon$.

The obtained closed formulae for the D_T are summarized in Table 1, considering the three classical cases of boundary conditions on the holes.

Table 1: **Analytical expressions for D_T depending on the b.c. applied on the holes**

B. C. Type	$D_T(\widehat{x})$	$\widehat{x}$
Neumann ($\alpha = 0, \beta = 1, \gamma = 0$)	$k\nabla u\nabla u - bu$	$\widehat{x} \in \Omega \cup \Gamma$
	$-q_\varepsilon u$	$\widehat{x} \in \Omega \cup \Gamma$
Dirichlet ($\alpha = 1, \beta = 0, \gamma = 0$)	$-\frac{1}{2}k(u - \overline{u}_\varepsilon)$	$\widehat{x} \in \Omega$
	$k\nabla u\nabla u - b\overline{u}_\varepsilon$	$\widehat{x} \in \Gamma$
Robin ($\alpha = 0, \beta = 0, \gamma = 1$)	$h_c^\varepsilon(u_\varepsilon - 2u_{\varepsilon\infty})$	$\widehat{x} \in \Omega \cup \Gamma$

*It is important to take attention that D_T is evaluated by different expressions for interior and boundary points.
**Topological optimization considering anisotropic media for potential problems were considered in Anflor and Marczak [2009].

2.2   Linear elasticity

The direct problem for elasticity is stated as,

$$\text{Find: } \{u_\epsilon | div\sigma_\varepsilon = b\} \text{ on } \Omega_\varepsilon \tag{15}$$

A general form for the cost function can be written as the total strain energy function:

$$\Psi(u_\tau) = \frac{1}{2}\int_{\Omega_\tau} C\nabla_\tau u_\tau \cdot \nabla_\tau u_\tau d\Omega_\tau - \int b \cdot u_\tau d\Omega_\tau - \int_\Gamma \bar{t} \cdot u_\tau d\tau = \frac{1}{2}a_\tau(u_\tau, u_\tau) - l_\tau(u_\tau), \tag{16}$$

where τ is the perturbation form for the cost function with respect to the shape, C is Hookeâs tensor, b is the body force, $\bar{t}$ is the traction boundary condition, and u_τ denotes the displacement vector field. Equation (17) refers to the sensitivity of the cost function with respect to τ and can be obtained from the *Gâteaux* derivative of the perturbed configuration given by Equation (13):

$$\frac{d}{d\tau}\Psi(\Omega_\tau)_{\tau=0} = \lim_{\tau \to 0}\frac{d}{d\tau}\Psi(\Omega_\tau). \tag{17}$$

In the absence of body forces, the D_T results:

$$D_T(\hat{x}) = -\lim_{\epsilon \to 0}\frac{1}{f'(\varepsilon)}\int_{\Gamma\varepsilon}\frac{1}{2\rho E}\sigma_\varepsilon^{tt} d\Gamma_\varepsilon. \tag{18}$$

If the limit of $\varepsilon \to 0$ in Equation 16, eq. 18 results:

$$D_T(\hat{x}) = \frac{1}{2\rho E}[(\sigma_1 + \sigma_2)^2 + 2(\sigma_1 - \sigma_2)^2], \tag{19}$$

where σ_1, σ_2 are the principal stresses of the stress tensor $\sigma|\hat{x}$ computed in $\hat{x} \; \epsilon \; \omega$. The principal stresses are given by

$$\sigma_{1,2} = \frac{1}{2}[tr\sigma \pm \sqrt{2\sigma^D \sigma^D}], \tag{20}$$

and σ^D is the deviatoric stress tensor:

$$\sigma^D = \sigma - \frac{1}{2}tr(\sigma)I. \tag{21}$$

Computing σ_1, σ_2 using Equations 20 and 21 and substituting in Equation 19 results in

$$D_T(\hat{x}) = \frac{1}{2\rho E}[4\sigma\sigma - (tr\sigma)^2]). \tag{22}$$

After some algebraic manipulation using Equation (19) and the constitutive relation, the D_T for plane stress problems stands as

$$D_T(\hat{x}) = \frac{2}{1+\nu}\sigma \cdot \varepsilon + \frac{(3\nu - 1)}{2(1-\nu^2)}\, tr\sigma \, tr\varepsilon \tag{23}$$

In eq.23, σ and ϵ are computed in the original domain, i.e. without voids. For the plane strain, the D_T results as

$$D_T(\hat{x}) = 2(1-\nu)\sigma \cdot \varepsilon + \frac{(1-\nu)(4\nu - 1)}{2(1-2\nu)}tr\sigma \, tr\varepsilon, \tag{24}$$

where ν denotes the Poisson ratio, while $tr\sigma$ and $tr\epsilon$ stand for the trace of the stress and strain tensors, respectively. A complete derivation for obtaining Equations 23 and 24 can be found in Novotny and Sokolowski [2013].

3 Topological Derivative considering the insertion of inclusions

In this section, the mathematical models for the diffusive-convective-reactive problem, Heat Exchanger, Eigenvalue of the Laplace problem, Kirchhoff Plate, Reissner-Mindlin Plate and Compliance. The original unperturbed and topologically perturbed problems are stated as well as the topological derivatives associate the shape functionals we are dealing with, are introduced.

3.1 Diffusive-Convective-Reactive Problem

The mathematical model for the diffusive-convective-reactive problem, as well as the shape functionals we are dealing with, are introduced. The original unperturbed and topologically perturbed problems are stated, together with arguments on the existence of the associated topological derivative (see Carvalho [2020]).

The original unperturbed problem is stated as:

$$u \in H_0^1(\Omega) : \int_\Omega \alpha \nabla u \cdot \nabla \eta + \int_\Omega \beta(\nabla u \cdot V)\eta + \int_\Omega \rho k u \eta = \int_\Omega f\eta \quad \forall \eta \in H_0^1(\Omega), \tag{25}$$

where α, β, ρ and k are positive and bounded functions, f is a distributed source and V is a given vector field, such that, $\text{div}(V) = 0$ in Ω and $V \cdot n = 0$ on $\partial\Omega$. The quantities α, β, ρ, k and f are assumed to be piecewise constant functions as described in Table 2, with $\omega \subset \Omega$. Precise physical meaning of (25) is given in Sections 3.1.2 and 3.1.3.

Table 2: **Values of α, β, ρ and f**

	α	β	ρ	f
$\Omega \setminus \omega$	α_0	β_0	ρ_0	f_0
ω	α_1	β_1	ρ_1	f_1

In Figure 2 is presented a scheme in which it is possible to remove or add material according to the domain sensitivity.
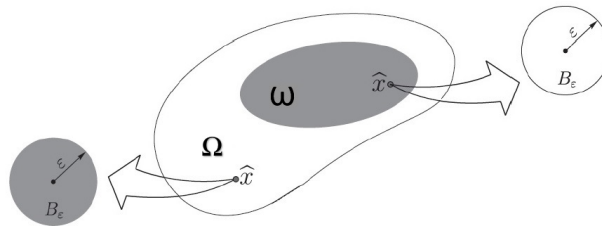
Figure 2: scheme of adding/removal material

The auxiliaries shape functionals are defined by,

$$\mathcal{G}(u) = \int_\Omega \rho k u^2 \qquad \text{and} \qquad \mathcal{J}(u) = \int_\Omega \alpha \|\nabla u\|^2. \tag{26}$$

In order to simplify further analysis, we introduce the adjoint problems

$$q \in H_0^1(\Omega) : \int_\Omega \alpha \nabla q \cdot \nabla \eta - \int_\Omega \beta (\nabla q \cdot V) \eta + \int_\Omega \rho k q \eta =$$
$$-2 \int_\Omega \rho k u \eta, \quad \forall \eta \in H_0^1(\Omega), \tag{27}$$

$$p \in H_0^1(\Omega) : \int_\Omega \alpha \nabla p \cdot \nabla \eta - \int_\Omega \beta (\nabla p \cdot V) \eta + \int_\Omega \rho k p \eta =$$
$$-2 \int_\Omega \alpha \nabla u \cdot \nabla \eta, \quad \forall \eta \in H_0^1(\Omega). \tag{28}$$

3.1.1 Perturbed problem

The topological perturbation is defined according to Tables **??** and 4, where $B_\varepsilon(\widehat{x}) = \{\|x - \widehat{x}\| < \varepsilon\}$ for $\widehat{x} \in \Omega$ and $\omega \subset \Omega$. From these elements, the topologically

perturbed problem is stated as,

$$u_\varepsilon \in H_0^1(\Omega) : \int_\Omega \alpha_\varepsilon \nabla u_\varepsilon \cdot \nabla \eta + \int_\Omega \beta_\varepsilon (\nabla u_\varepsilon \cdot V)\eta + \int_\Omega \rho_\varepsilon k u_\varepsilon \eta =$$

$$\int_\Omega f_\varepsilon \eta \quad \forall \eta \in H_0^1(\Omega), \quad (29)$$

with $V \cdot n = 0$ on ∂B_ε. The auxiliary shape functionals in perturbed domain are defined by

$$\mathcal{G}_\varepsilon(u_\varepsilon) = \int_\Omega \rho_\varepsilon k u_\varepsilon^2 \quad \text{and} \quad \mathcal{J}_\varepsilon(u_\varepsilon) = \int_\Omega \alpha_\varepsilon \|\nabla u_\varepsilon\|^2. \quad (30)$$

The contrasts of materials in the perturbed domain are shown in the tables 3 and 4.

Table 3: Values of α_ε, β_ε, ρ_ε and f_ε

	α_ε	β_ε	ρ_ε	f_ε
$\Omega \setminus B_\varepsilon$	α	β	ρ	f
B_ε	$\gamma_\alpha \alpha$	$\gamma_\beta \beta$	$\gamma_\rho \rho$	$\gamma_f f$

Table 4: Values of γ_α, γ_β, γ_ρ and γ_f

	γ_α	γ_β	γ_ρ	γ_f
$\Omega \setminus \omega$	α_1/α_0	β_1/β_0	ρ_1/ρ_0	f_1/f_0
ω	α_0/α_1	β_0/β_1	ρ_0/ρ_1	f_0/f_1

Before stating the two main results, let us introduce the following second-order polarization tensors

$$\mathbf{P}_\alpha = \frac{1 - \gamma_\alpha}{1 + \gamma_\alpha}\mathbf{I} \quad \text{and} \quad \mathbf{P}_{\alpha\beta} = \frac{1 - \gamma_\beta}{1 + \gamma_\alpha}\mathbf{I}, \quad (31)$$

associated with the contrast on the diffusive γ_α and convective γ_β terms. From the problems presented in (25) and (29) two results are formulated, related to the topological derivative.

Theorem 1 *Let $\mathcal{G}(u)$ be the shape functional defined in (26)-left, then its associated topological derivative is given by*

$$D_T\mathcal{G} = -2\alpha\mathbf{P}_\alpha\nabla u \cdot \nabla q - 2\beta(\mathbf{P}_{\alpha\beta}\nabla u \cdot V)q - \rho k(1 - \gamma_\rho)u(u + q) + (1 - \gamma_f)qf, \quad (32)$$

where q is the adjoint state solution of (27).

Theorem 2 *Let $\mathcal{J}(u)$ be the shape functional presented in (26)-right. Then, the topological derivative of $\mathcal{J}$ is given by*

$$D_T\mathcal{J} = -2\alpha\mathbf{P}_\alpha\nabla u \cdot \nabla(u + p) - 2\beta(\mathbf{P}_{\alpha\beta}\nabla u \cdot V)p - \rho k(1 - \gamma_\rho)up + (1 - \gamma_f)pf, \quad (33)$$

where p is the adjoint solution of problem (28).

3.1.2   Heat Exchanger

We are interested in the diffusion-convection (Eq. (25) with $k = 0$) problem which can be stated as: Find u, such that

$$\begin{cases} -\text{div}(\alpha\nabla u) + \beta(\nabla u \cdot V) &= f \quad \text{in} \quad \Omega\,, \\ u &= 0 \quad \text{on} \quad \Gamma_D, \\ \partial_n u &= 0 \quad \text{on} \quad \Gamma_N. \end{cases} \tag{34}$$

Therefore, u represents the temperature field, whereas α is the diffusion coefficient, β is the convection coefficient and V is a given velocity field.

Let us consider the following shape functional

$$\mathcal{F}(u) = \tau \int_\Omega \alpha\|\nabla u\|^2 + (1-\tau)\int_\Omega \rho|u|^2, \tag{35}$$

with $0 \le \tau \le 1$ and u solution to (34). Then, its associated topological derivative, by taking into account contrasts on α and ρ (and not on β as well as on f), is given by (see Ruscheinsky et al. [2020b]),

$$D_T\mathcal{F} = -2\alpha\mathbf{P}_\alpha\nabla u \cdot (\tau\nabla u + \nabla p + \nabla q) - (1-\tau)(1-\gamma_\rho)\rho|u|^2, \tag{36}$$

where p and q are respectively solutions of the following adjoint problems

$$p \in \mathcal{U}(\Omega): \int_\Omega \alpha\nabla p \cdot \nabla\eta - \int_\Omega (\nabla p \cdot V)\eta = -2\tau\int_\Omega \alpha\nabla u \cdot \nabla\eta \quad \forall\eta \in \mathcal{U}(\Omega), \tag{37}$$

$$q \in \mathcal{U}(\Omega): \int_\Omega \alpha\nabla q \cdot \nabla\eta - \int_\Omega (\nabla q \cdot V)\eta = -2(1-\tau)\int_\Omega \rho u\eta \quad \forall\eta \in \mathcal{U}(\Omega), \tag{38}$$

with the space $\mathcal{U}(\Omega) = \{\varphi \in H^1(\Omega): \varphi_{|\Gamma_D} = 0\}$.

3.1.3   Eigenvalue of the Laplace problem

The eigenvalue of the Laplace problem modeling a membrane under free vibration can be stated as: Find u and λ, such that

$$\begin{cases} -\text{div}(\alpha\nabla u) &= \lambda\rho u \quad \text{in} \quad \Omega, \\ u &= 0 \quad\quad \text{on} \quad \partial\Omega, \end{cases} \tag{39}$$

so that u represents the transverse displacement field, α is the stiffness coefficient and ρ is the density.

The associated first eigenvalue is defined as

$$\lambda_1 = \frac{\int_\Omega \alpha\|\nabla u\|^2}{\int_\Omega \rho|u|^2}, \tag{40}$$

with u solution of (39). The topological derivative for simple eigenvalues of the Laplacian can be found in Ammari and Khelifi [2003]. The extension to multiple eigenvalues and other types of singular domain perturbations has been derived in Nazarov and Sokolowski [2008]. In particular, the topological derivative of

$$\mathcal{F}(u) = \lambda_1^{-1} \tag{41}$$

is given by:

$$D_T\mathcal{F} = \frac{2\alpha\mathbf{P}_\alpha\nabla u \cdot \nabla u - (1-\gamma_\rho)\rho\lambda_1|u|^2}{\lambda_1^2 \int_\Omega \rho|u|^2}, \tag{42}$$

which can be formally derived from Theorems 1 and 2. The rigorous justification for this result can be found in the book by Novotny and Sokolowski [2013]. As observed by Haftka and Gürdal [1992], standard sensitivities of eigenvalues hold only in the case of distinct eigenvalues. According to Seyranian et al. [1994] symmetric and complex structures that depend on many design parameters often present multiple eigenvalues. A numerical method of solution was developed by the authors to determine an ascent direction in the design space for the smallest eigenvalue. More recently, a simple strategy proposed by Zhang et al. [2015] can be used in order to deal with multiplicity of eigenmodes, which consists in select the closest eigenmode to the current one. See also the paper by Torii and Rocha de Faria [2017] for more sophisticated approach based on a smooth p-norm approximation for the smallest eigenvalue.

3.2   Kirchhoff Plates

Before starting the main results of this section, let us introduce the following fourth-order polarization tensor associated with the plate bending model

$$\mathbb{P} = -\frac{1-\gamma_\alpha}{1+\gamma_\alpha\delta_2}\left((1+\delta_2)\mathbb{I} + \frac{1-\gamma_\alpha}{2}\frac{\delta_1-\delta_2}{1+\gamma_\alpha\delta_1}\mathrm{I}\otimes\mathrm{I}\right), \tag{43}$$

where constants δ_1 and δ_2 will be defined later according to the model problem we are dealing with, namely Kirchhoff or Reissner-Mindlin. In (43), the symbols I and $\mathbb{I}$ are used to denote the second and fourth order identity tensors, respectively

The theory of Kirchhoff bending plates is based on the following kinematic assumption:

> *The normal fibers to the middle plane of the plate remain normal during deformation and do not suffer variations in their length. Consequently, both transversal shear and normal deformations are null.*

Therefore, the original unperturbed problem can be stated as: Find $u \in \mathcal{V}(\Omega)$, such that

$$\int_\Omega \alpha M(u) \cdot \nabla\nabla v + \int_\Omega \rho k u v = \int_\Omega f v, \quad \forall v \in \mathcal{V}(\Omega), \tag{44}$$

where $\mathcal{V}(\Omega) = H_0^2(\Omega;R)$. The coefficients α, ρ and f are given in Table 5. In addition, $M(u) = \mathbb{C}\nabla\nabla u$ is the moment tensor, $u : \Omega \mapsto R$ the transverse displacement and k a positive function. The constitutive tensor $\mathbb{C}$ is given by

$$\mathbb{C} = \frac{Eh^3}{12(1-\nu^2)}\left((1-\nu)\mathbb{I} + \nu\mathrm{I}\otimes\mathrm{I}\right), \tag{45}$$

being ν is the Poisson ratio, E is the Young modulus and h the plate thickness. The L^2 and energy norms shape functionals, we are dealing with, are respectively defined as

$$\mathcal{G}(u) = \int_\Omega \rho k|u|^2 \quad \text{and} \quad \mathcal{J}(u) = \int_\Omega \alpha M(u) \cdot \nabla\nabla u. \tag{46}$$

In order to simplify bluethe form of the topological derivatives, we introduce the adjoint problems for displacements q and p, as

$$q \in \mathcal{V}(\Omega) : \int_\Omega \alpha M(q) \cdot \nabla\nabla v + \int_\Omega \rho k q v = -2 \int_\Omega \rho k u v, \quad \forall v \in \mathcal{V}(\Omega), \quad (47)$$

$$p \in \mathcal{V}(\Omega) : \int_\Omega \alpha M(p) \cdot \nabla\nabla v + \int_\Omega \rho k p v = -2 \int_\Omega \alpha M(u) \cdot \nabla\nabla v, \quad \forall v \in \mathcal{V}(\Omega). \quad (48)$$

The topologically perturbed counterpart of problem (44) is written as: Find $u_\varepsilon \in \mathcal{V}(\Omega)$, such that

$$\int_\Omega \alpha_\varepsilon M(u_\varepsilon) \cdot \nabla\nabla v + \int_\Omega \rho_\varepsilon k u_\varepsilon v = \int_\Omega f_\varepsilon v, \quad \forall v \in \mathcal{V}(\Omega), \quad (49)$$

where the coefficients α_ε, ρ_ε and f_ε are defined through Table 3 and Table 4. The associated shape functionals are then defined as

$$\mathcal{G}_\varepsilon(u_\varepsilon) = \int_\Omega \rho_\varepsilon k |u_\varepsilon|^2 \quad \text{and} \quad \mathcal{J}_\varepsilon(u_\varepsilon) = \int_\Omega \alpha_\varepsilon M(u_\varepsilon) \cdot \nabla\nabla u_\varepsilon. \quad (50)$$

3.2.1   Topological sensitivities

By setting the constants δ_1 and δ_2 in the definition of the polarization tensor (43) as follows

$$\delta_1 = \frac{1+\nu}{1-\nu} \quad \text{and} \quad \delta_2 = \frac{1-\nu}{3+\nu}, \quad (51)$$

we can state the two main results of this Section, whose proofs are completely analogous to the presented by Amstutz and Novotny [2011]:

Theorem 3 *Let $\mathcal{G}(u)$ be the shape functional defined by (46)-left, then its associated topological derivative is given by*

$$D_T \mathcal{G} = \alpha \mathbb{P} M(u) \cdot \nabla\nabla q - (1-\gamma_\rho)\rho k u (u+q) + (1-\gamma_f) f q \quad \text{a.e. in } \Omega \quad (52)$$

where q is the adjoint state solution of (47).

Theorem 4 *Let $\mathcal{J}(u)$ be the shape functional presented in (46)-right, then its topological derivative is given by*

$$D_T \mathcal{J} = \alpha \mathbb{P} M(u) \cdot \nabla\nabla(u+p) - (1-\gamma_\rho)\rho k u p + (1-\gamma_f) f p \quad \text{a.e. in } \Omega \quad (53)$$

where p is the adjoint solution of problem (48).

The eigenvalue problem for the Kirchhoff model of a clamped thin plate under free vibration can be stated as: Find u and λ, such that

$$\begin{cases} \operatorname{div}\operatorname{div}(\alpha M(u)) &= \lambda \rho u \quad \text{in} \quad \Omega, \\ u = \partial_n u &= 0 \quad \text{on} \quad \partial\Omega. \end{cases} \quad (54)$$

The associated first eigenvalue can be defined as

$$\lambda_1 = \frac{\int_\Omega \alpha M(u) \cdot \nabla \nabla u}{\int_\Omega \rho |u|^2}, \tag{55}$$

being u solution of (54). The topological derivative of $J(\mathcal{D}) := \lambda_1^{-1}$ is given by (see Carvalho et al. [2020]),

$$D_T J = -\frac{\alpha \mathbb{P} M(u) \cdot \nabla \nabla u + (1 - \gamma_\rho) \rho \lambda_1 |u|^2}{\lambda_1^2 \int_\Omega \rho |u|^2}. \tag{56}$$

3.3   Reissner-Mindlin Plates

The theory of Reissner-Mindlin bending plates is based on the following kinematic assumption:

> *The normal fibers to the middle plane of the plate remain straight during the deformation process and do not suffer variations in their length, but they do not necessarily remain normal to the middle plane. Consequently, the transversal shear deformations are not negligible and the normal deformations are null.*

Therefore, the unperturbed problem is stated as: Find $(\theta, u) \in \mathcal{H}(\Omega)$, such that

$$\int_\Omega \alpha M(\theta) \cdot (\nabla \eta)^s + \int_\Omega \beta Q(\theta, u) \cdot (\eta - \nabla v) + \int_\Omega \rho k u v = \int_\Omega f v, \quad \forall (\eta, v) \in \mathcal{H}(\Omega), \tag{57}$$

where $\mathcal{H}(\Omega) = H_0^1(\Omega; R^2) \times H_0^1(\Omega; R)$. The coefficients α, β, ρ and f are given in Table 2. In addition, $\theta : \Omega \mapsto R^2$ is the rotation, $u : \Omega \mapsto R$ is the transversal displacement, $M(\theta) = \mathbb{C}(\nabla \theta)^s$ is the generalized bending moment tensor and $Q(\theta, u) = D(\theta - \nabla u)$ is the generalized shear tensor. The constitutive tensor $\mathbb{C}$ is defined by (45) whereas the second order tensor D is given by

$$D = \frac{\sigma E h}{2(1 + \nu)} \mathrm{I}, \tag{58}$$

with shear correction factor $\sigma = 5/6$. The L^2 and energy norms shape functionals, we are dealing with, are defined as

$$\mathcal{G}(\theta, u) = \int_\Omega \rho k |u|^2 \quad \text{and} \quad \mathcal{J}(\theta, u) = \int_\Omega (\alpha M(\theta) \cdot (\nabla \theta)^s + \beta Q(\theta, u) \cdot (\theta - \nabla u)). \tag{59}$$

In order to simplify bluethe form of the topological derivatives, we introduce the adjoint problems for displacements (q, p) and the rotations (φ, ϕ), as

$$(\varphi, q) \in \mathcal{H}(\Omega) : \int_\Omega \alpha M(\varphi) \cdot (\nabla \eta)^s + \int_\Omega \beta Q(\varphi, q) \cdot (\eta - \nabla v) + \int_\Omega \rho k q v =$$
$$- 2 \int_\Omega \rho k u v, \quad \forall (\eta, v) \in \mathcal{H}(\Omega), \tag{60}$$

$$(\phi, p) \in \mathcal{H}(\Omega) : \int_\Omega \alpha M(\phi) \cdot (\nabla \eta)^s + \int_\Omega \beta Q(\phi, p) \cdot (\eta - \nabla v) + \int_\Omega \rho k p v =$$

$$- 2 \int_\Omega (\alpha M(\theta) \cdot (\nabla \eta)^s + \beta Q(\theta, u) \cdot (\eta - \nabla v)), \quad \forall (\eta, v) \in \mathcal{H}(\Omega). \quad (61)$$

The topologically perturbed counterpart of problem (57) is written as: Find $(\theta_\varepsilon, u_\varepsilon) \in \mathcal{H}(\Omega)$, such that

$$\int_\Omega \alpha_\varepsilon M(\theta_\varepsilon) \cdot (\nabla \eta)^s + \int_\Omega \beta_\varepsilon Q(\theta_\varepsilon, u_\varepsilon) \cdot (\eta - \nabla v) + \int_\Omega \rho_\varepsilon k u_\varepsilon v = \int_\Omega f_\varepsilon v, \quad \forall (\eta, v) \in \mathcal{H}(\Omega),$$

$$(62)$$

where the coefficients α_ε, β_ε, ρ_ε and f_ε are reported in Tables **??** and 4. The associated shape functionals are then defined as

$$\mathcal{G}_\varepsilon(\theta_\varepsilon, u_\varepsilon) = \int_\Omega \rho_\varepsilon k |u_\varepsilon|^2 \quad \text{and} \quad (63)$$

$$\mathcal{J}_\varepsilon(\theta_\varepsilon, u_\varepsilon) = \int_\Omega (\alpha_\varepsilon M(\theta_\varepsilon) \cdot (\nabla \theta_\varepsilon)^s + \beta_\varepsilon Q(\theta_\varepsilon, u_\varepsilon) \cdot (\theta_\varepsilon - \nabla u_\varepsilon)). \quad (64)$$

3.3.1 Topological sensitivities

Let us introduce the following second-order tensor

$$P = -2 \frac{1 - \gamma_\beta}{1 + \gamma_\beta} \, \mathrm{I}. \quad (65)$$

Now, by setting the constants δ_1 and δ_2 in the definition of the polarization tensor (43) as follows

$$\delta_1 = \frac{1 + \nu}{1 - \nu} \quad \text{and} \quad \delta_2 = \frac{3 - \nu}{1 + \nu}, \quad (66)$$

we can state the two main results of this section, whose proofs are completely analogous to the paper by Sales et al. [2015]:

Theorem 5 *Let $\mathcal{G}(\theta, u)$ be the shape functional defined by (59)-left, then its associated topological derivative is given by*

$$D_T \mathcal{G} = \alpha \mathbb{P} M(\theta) \cdot (\nabla \varphi)^s + \beta P Q(\theta, u) \cdot (\varphi - \nabla q)$$
$$- (1 - \gamma_\rho) \rho k u (u + q) + (1 - \gamma_f) f q \quad a.e. \ in \ \Omega \quad (67)$$

where (φ, q) is the adjoint state solution of (60).

Theorem 6 *Let $\mathcal{J}(\theta, u)$ be the shape functional presented in (59)-right, then its associated topological derivative is given by*

$$D_T \mathcal{J} = \alpha \mathbb{P} M(\theta) \cdot (\nabla(\theta + \phi))^s + \beta P Q(\theta, u) \cdot ((\theta + \phi) - \nabla(u + p))$$
$$- (1 - \gamma_\rho) \rho k u p + (1 - \gamma_f) f p \quad a.e. \ in \ \Omega \quad (68)$$

where (ϕ, p) is the adjoint solution of problem (61).

the eigenvalue problem of a Reissner-Mindlin model of a clamped thick plate under free vibration can be stated as: Find (θ, u) and λ, such that

$$
\begin{cases}
-\text{div}(\alpha M(\theta)) + \beta Q(\theta, u) & = & 0 & \text{in} & \Omega\,, \\
\text{div}(\beta Q(\theta, u)) & = & \rho\lambda u & \text{in} & \Omega\,, \\
\theta = 0,\ u & = & 0 & \text{on} & \partial\Omega\,.
\end{cases}
\tag{69}
$$

The associated first eigenvalue is defined as

$$
\lambda_1 = \frac{\int_\Omega (\alpha M(\theta) \cdot (\nabla\theta)^s + \beta Q(\theta, u) \cdot (\theta - \nabla u))}{\int_\Omega \rho|u|^2},
\tag{70}
$$

being (θ, u) solution of (69). The topological derivative of $J(\mathcal{D}) = \lambda_1^{-1}$ is given by (see Carvalho et al. [2020]),

$$
D_T J = -\frac{\alpha \mathbb{P} M(\theta) \cdot (\nabla\theta)^s + \beta P Q(\theta, u) \cdot (\theta - \nabla u) + (1 - \gamma_\rho)\rho\lambda_1|u|^2}{\lambda_1^2 \int_\Omega \rho|u|^2}.
\tag{71}
$$

3.4   Compliance Problem

The compliance of the plate under bending effects is obtained as the sum of the shape functionals given by (46) for Kirchhoff problem and by (59) for Reissner-Mindlin problem. The zero order term in both problems (see eqs. (44) and (57)) can be interpreted as an elastic support, so that we define the quantity $s = \rho k$, where s represents the stiffness of the support. The transverse load f is assumed to be fixed, so that its associated contrast $\gamma_f = 1$.

In the case of Kirchhoff plate bending problem, the shape functional to be minimized is defined as $J(\mathcal{D}) := \mathcal{J}(u) + \mathcal{G}(u)$, with $\mathcal{J}(u)$ and $\mathcal{G}(u)$ given by (46), where u is the solution to: Find u, such that

$$
\begin{cases}
\text{div}\,\text{div}(\alpha M(u)) + su & = & f & \text{in} & \Omega, \\
u = \partial_n u & = & 0 & \text{on} & \partial\Omega.
\end{cases}
\tag{72}
$$

Therefore, from Theorem 3 and Theorem 4, we have that the associated topological derivative of the compliance shape functional $J(\mathcal{D})$ is given by (see, Carvalho et al. [2020]),

$$
D_T J = -\alpha \mathbb{P} M(u) \cdot \nabla\nabla u + (1 - \gamma_\rho)s|u|^2.
\tag{73}
$$

Analogously, in the case of Reissner-Mindlin plate bending problem, the shape functional to be minimized is defined as $J(\mathcal{D}) := \mathcal{J}(\theta, u) + \mathcal{G}(\theta, u)$, with $\mathcal{J}(\theta, u)$ and $\mathcal{G}(\theta, u)$ given by (59), where (θ, u) are the solutions to: Find (θ, u), such that

$$
\begin{cases}
-\text{div}(\alpha M(\theta)) + \beta Q(\theta, u) & = & 0 & \text{in} & \Omega\,, \\
\text{div}(\beta Q(\theta, u)) + su & = & f & \text{in} & \Omega\,, \\
\theta = 0,\ u & = & 0 & \text{on} & \partial\Omega\,.
\end{cases}
\tag{74}
$$

Thus, from Theorem 5 and Theorem 6, we have that the associated topological derivative of the compliance shape functional $J(\mathcal{D})$ is given by

$$
D_T J = -\alpha \mathbb{P} M(\theta) \cdot (\nabla\theta)^s - \beta P Q(\theta, u) \cdot (\theta - \nabla u) + (1 - \gamma_\rho)s|u|^2.
\tag{75}
$$

4   Numerical strategy framework

In this section the illustrative scheme presented in fig. 3 shows the numerical strategy implemented for the methodology aforementioned. The steps of implementation can be listed as,

- Step 1 - Generates the geometry, boundary conditions, and set the mechanical properties;

- Step 2 - Solves the direct problem using the chosen numerical solver (FEM, BEM, or other);

- Step 3 - Applies the respective D_T closed formula to the problem under consideration to get the domain's sensitivity;

- Step 4 - Select those points with low efficiency (low D_T) for being removed. Remark: The user must set the percentage of volume to be removed per iteration;

- Step 5 - Applies an auxiliary routine for material removal at the candidate internal points. Remark: This routine is based on pure geometry depending on the numerical method employed and must be able to detect new frontiers reapplying the b.c. as well as to detect the possible detached material (islands) from the main domain (mainly for BEM).
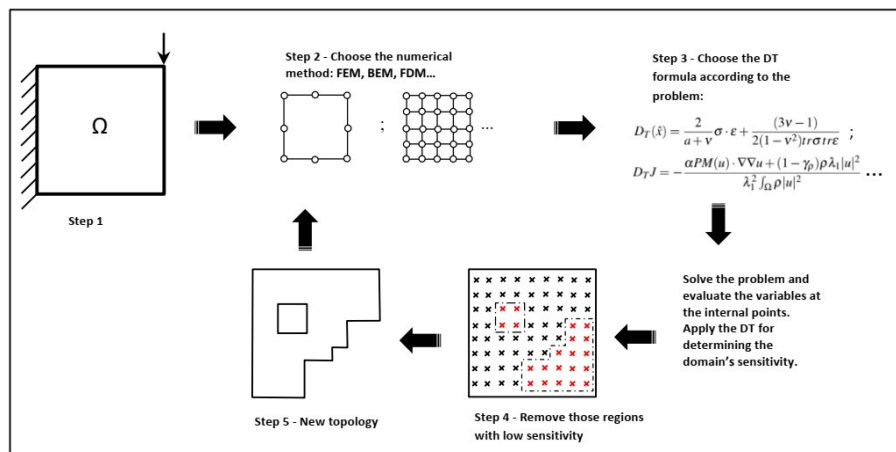
Figure 3: Numerical methodology scheme for implementation

It is important to highlight that the strategy of material removal depends on the numerical approach and the methodology employed by the user to deal with the geometry. In the case of FEM, generally, one can set the domain fixed and suppress (in case of voids) or impose different values of mechanical properties (in case of inclusion insertion) to those elements with low sensitivities. In this kind of approach, no concerns with the boundary conditions or even islands arising up are needed, because the elements are not rearranged, see for instance the work

of Ruscheinsky et al. [2020a]. It is also important to reinforce that the concept of D_T is derived considering the singular perturbation as voids or inclusions. In this sense, one must have attention to using the appropriate D_T closed formula to implement the strategy of removal/add material accordingly. When considering the BEM, one can deal with a fixed domain or moving frontiers. The first strategy is similar to the FEM procedure but in this case the technique of multiple regions must be considered, as implemented in Anflor et al. [2014]. For the moving frontiers, special treatment must be given in attention to the new geometry resulted from the previous iteration. When considering moving frontiers, the material is removed and new elements are added to redesign the domain needing the rearrangement on the discretization process. At this point, islands may arise (fig. 4 and the subroutine developed for Step 5, must be able to detect and discard them.
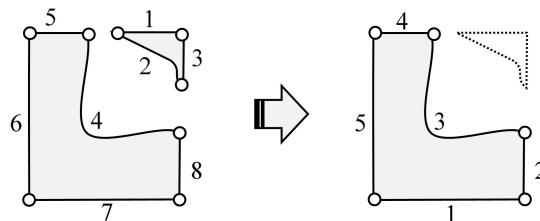
Figure 4: Detail of island detection, deletion and the renumbering of the elements

Additionally, several resources such as offset of internal points (switch off the entire grid of internal points), shape and size of stamps used to remove material are examples of strategies to improve in fast and efficiency of the iterative process when using BEM (fig.5). Further details about these strategies can be consulted in Marczak [2008] and Anflor et al. [2018].

Full grid of internal points   Off-set of internal points   New topology
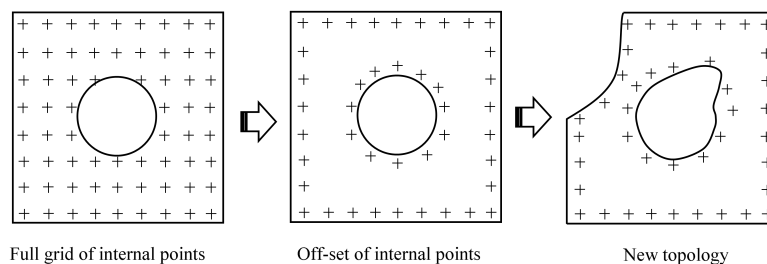
Figure 5: Strategies based on the BEM particularities

5   Numerical examples

This section presents some numerical examples in the context of topological optimization for classical problems of engineering, such as: Potential Problem,

Linear Elasticity, Heat Exchanger, Maximization of the First Eigenvalue in Membrane, Plates (Kirchhoff and Reissner-Mindlin) and the Compliance for Kirchhoff and Reissner-Mindlin problem. The algorithm based on the D_T is implemented using BEM for the first two examples and FEM for the remaining examples. The resulting analytical formulae (see formulas (36), (42), (56),(71), (73), (75)) are used together with a level-set domain representation method to devise a simple topology design algorithm (for more details see Amstutz and Andrä [2006]). The obtained final topologies show the efficiency of the topological derivative method.

5.1   Potential Problem: Printed Circuit Board

This example concerns to a printed circuit board (PCB) substrate. The characteristics of of good PCB designs is the efficiency to dissipate the maximum amount of thermal energy with the minimum possible volume of material. In this sense the topology optimization becomes attractive for this class of problem. Figure 6 introduces the initial layout for this case, where four heat sources are used to simulate the heat generated by major electronic components mounted on the PCB. The hatched areas are not allowed changes because they are used for clamping the PCB. The domain is discretized with 32 linear boundary elements (BEs) and the holes opened during the optimization process with 6 linear BEs. All the cavities opened as the iterative process evolves have prescribed Neumann homogeneous as boundary condition. For this problem the optimization procedure is halted was halted when a volume ratio of 70% between the final and the original designs is achieved. The domain's sensitivity was computed using the first equation introduced in Table 1. The evolution history is introduced according Fig. 7. It is worth mentioning that in the PCB case, new cavities are created during the process near the corners, characterizing truly topological changes in the domain.
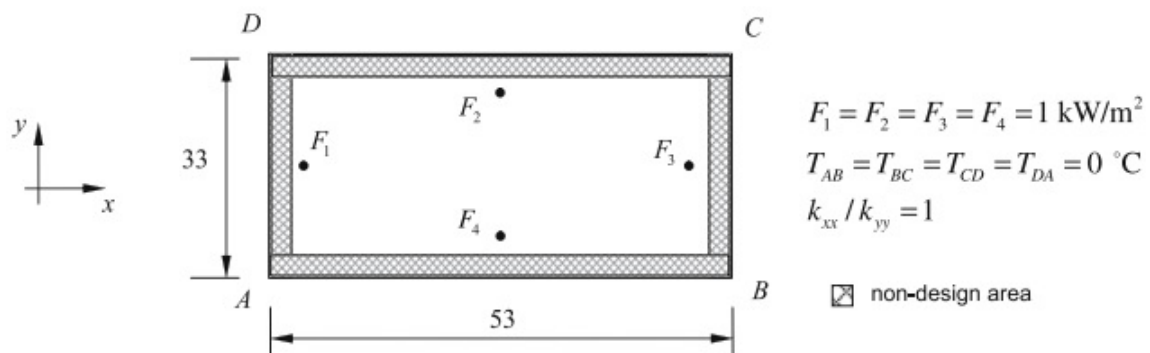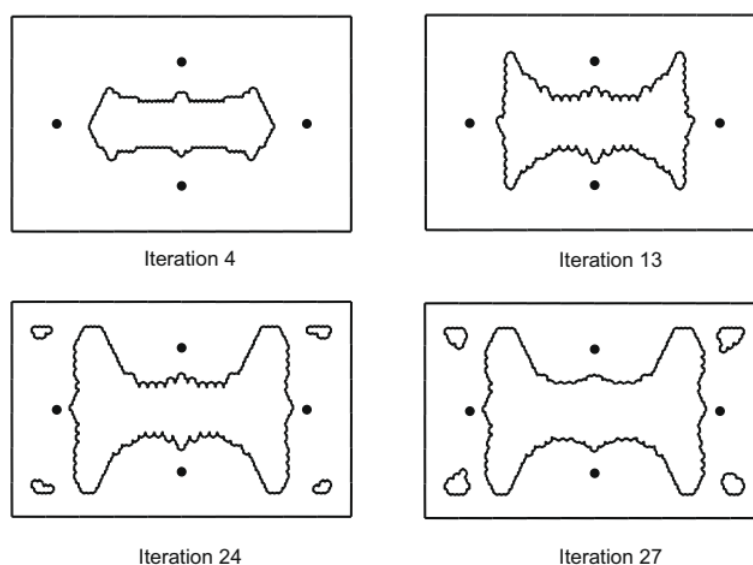

Figure 6: Initial design for the PCB

Figure 7: Topology evolution for the PCB

5.2 Linear Elasticity

This example consists of a traditional beam, as shown in 8. A rectangle with dimensions of 5 units x 10 units is subjected to a total vertical load P = 1 kN applied at the middle of the bottom side. The first and the last element of the bottom side are pinned and bolted, respectively. The radius of the holes was set to 0.013125a. The stop criterion was set as the final volume reaching approximately 54% of the initial volume and the domain's sensitivity was computed using eq.23. The percentages of internal points selected to be removed during the optimization procedure are presented in Table 1. As can be seen, the amount of material removed during the iterative process is variable, based on the domain's sensitivity. As a comparison, the amount of material removed using linear and quadratic BEs is also presented. Figure 6 shows the evolution of the iterative process using quadratic elements, where the final topology results after only six iterations. The final topology results for linear and quadratic BEs are quite similar, as expected. The main difference is that with increasing accuracy of the BE solutions, the domain sensitivity isolines become more evident, allowing the removal of a greater amount of material per iteration.

It is important to highlight that the final topology resulted in the shape of a truss structure, as shown in Figure 9. Using a mirror-image effect procedure on this final topology (iteration 6), the result is a geometry similar to a wheel with radial supports (Figure 11). Based on the literature, a resulting shape of a wheel ensures that the developed optimization routine is capable of generating feasible topologies. In Figure 10 it is possible to observe the amount of material being removed, taking into account the linear and quadratic BEs, as the iterative process evolves.
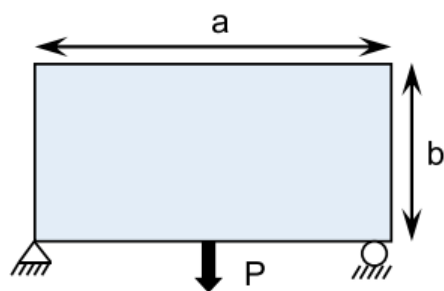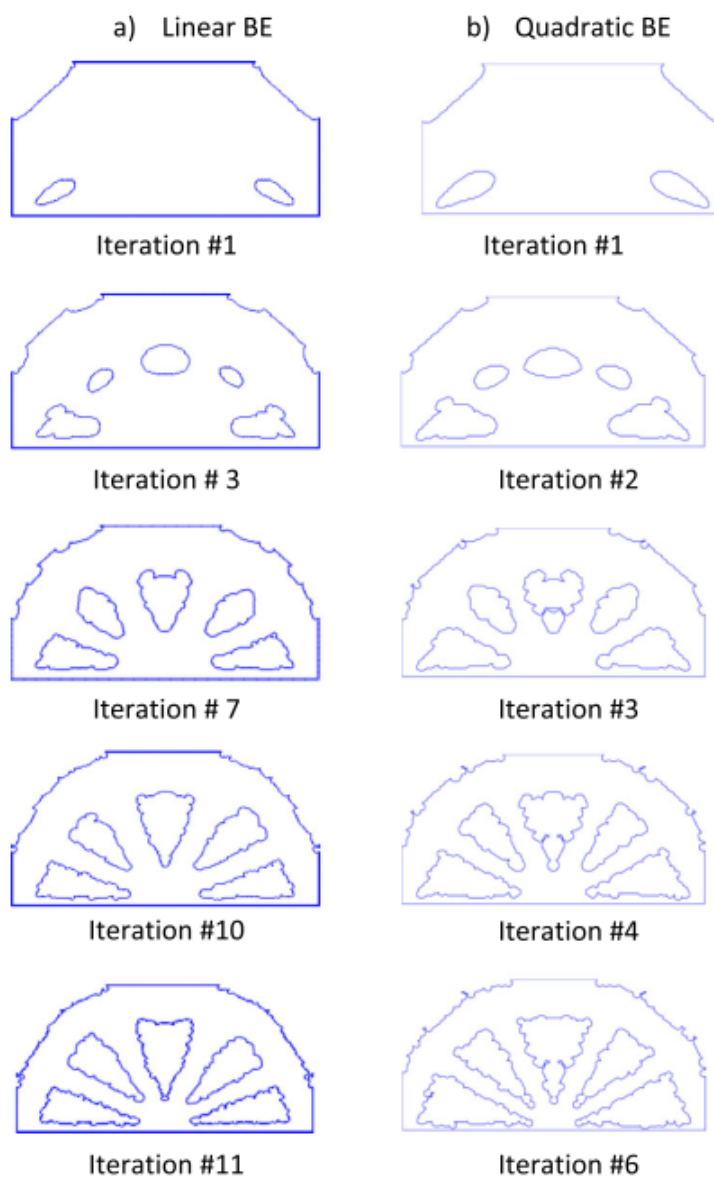
Figure 8: Beam boundary conditions

Figure 9: Beam topology evolution: a) linear and b) quadratic boundary elements
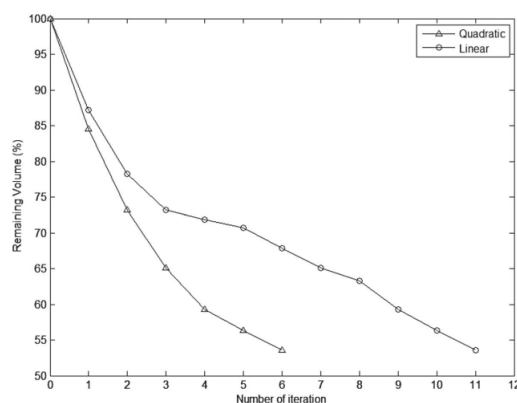
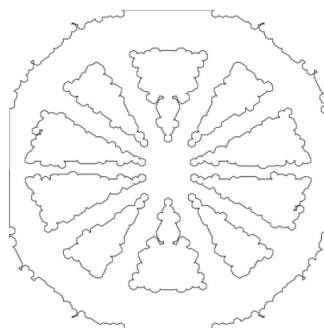**Figure 10: Volume x number of iterations history**

Figure 11: Final topology after a mirror-image effect

5.3 Heat Exchanger Design

The hold-all domain $\mathcal{D}$ is given by a unit square of size $(0, 1) \times (0, 1)$ with a distributed uniform heat generation of intensity $f = 10^4\,W$ over the domain. All the boundary are thermally insulated, with exception of the regions T_L and T_H of lengths 0.2. The temperature at T_L is prescribed as $u = 273\,K$ and T_H is prescribed as $u = 373\,K$. Fig. 12 shows the initial domain and the initial temperature map. The penalty parameter is set as $\mu = 4$, the weight as $t = 1$ and $\alpha = 1$. During the optimization procedure two material are used, the first one is the aluminum ($\alpha = 205W/mK$) and the second one is a material with low thermal conductivity $\gamma_\alpha \ll \alpha$. The initial domain consists of aluminum only ($\Omega = \mathcal{D}$). As the optimization process iterativelly evolves the aluminum is replaced by the second material. The domain's sensitivity is computed according to eq.36. Figures 13a-d show the evolution of topologies in the jth iteration. In the j=56 iteration, we have the optimized topology. Figure 14, illustrates the shape function. The final topology (see Fig. 13(d)) has 60% volume of high thermal conductivity material.
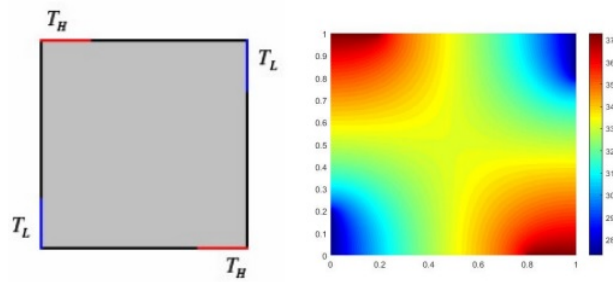
Figure 12: initial domain (left) and the initial temperature map (right)
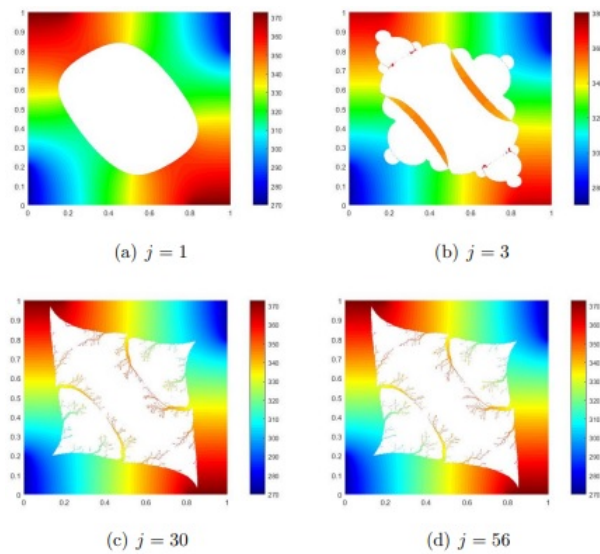

(a) $j = 1$ (b) $j = 3$

(c) $j = 30$ (d) $j = 56$

Figure 13: Topologies evolution (j^{th}) iteration (a)-(d) and Final topology (d)
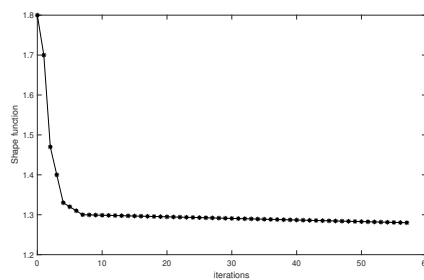

Figure 14: Shape function history

5.4 Membrane Problem: First eigenvalue maximization

The membrane is clamped in the four vertices and free in the rest of the contour. The non-structural concentrated mass m is applied at the plate's center $(0.5, 0.5)$, as depicted in Figure 15. Four cases are considered, namely, cases M1, M2, M3 and M4. The values of the penalty parameters μ and the non-structural mass m as

depicted in table 5. The domain's sensitivity is computed according to eq. 42.
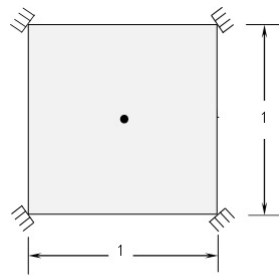
Figure 15: Initial domain

Table 5: Penalty values and concentrated mass

	Case M1	Case M2	Case M3	Case M4
μ	0.4	0.2	0.1	0.4
m	0.02	0.03	0.04	0.7

The final topologies for each case are presented in Figures 16a-d. Fig. 17 introduces the normalized first eigenvalue history λ_1/λ_0 (where λ_0^1 is its initial value) as the iterative process has evolved. The normalized first eigenvalues history λ_1/λ_2 are introduced in figure 18. Note that they are completely separated, so that multiple eigenvalues phenomenon was not observed in this particular example. The evolution histories for the volume fraction and shape funcion are presented in Fig. 19 and 20, respectively. The initial domain is discretized by using linear triangular finite elements resulting in an initial uniform mesh with 10,000 elements and 5,101 nodes. In order to increase the accuracy as well as the topology smoothness 4 steps of mesh refinement during the iterative process are allowed. After the fourth refinement the resulting mesh presents 2,560,000 elements and 1,281,601 nodes.

(a) Case M1   (b) Case M2   (c) Case M3   (d) Case M4
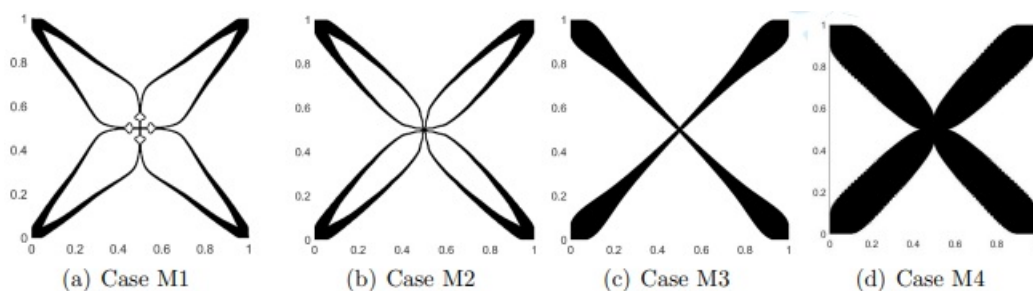
Figure 16: Optimized topologies for Cases M1, M2, M3 and M4

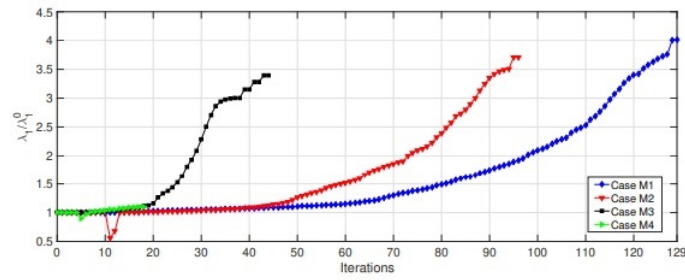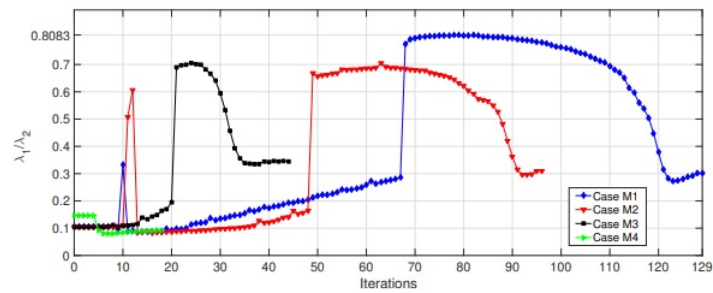**Figure 17: Normalized first eigenvalue λ_1/λ_1^0 history**

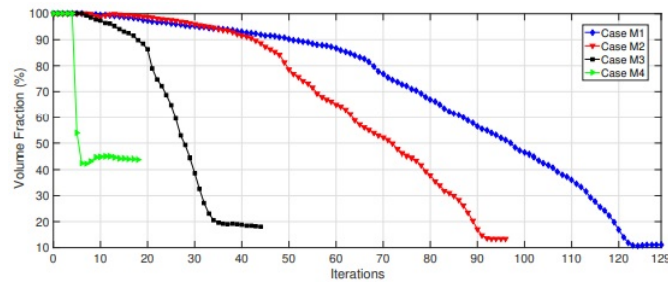**Figure 18: Normalized first eigenvalue λ_1/λ_2 history**

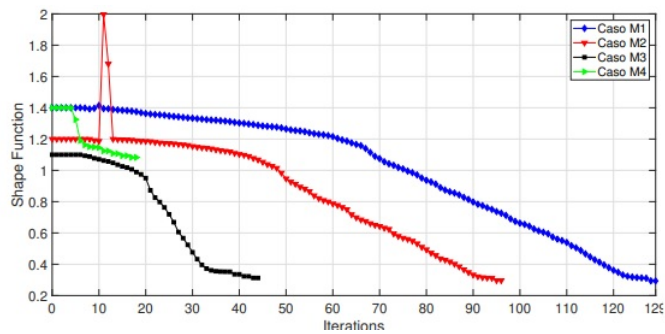**Figure 19: Shape Function history**

Figure 20: Volume Fraction history

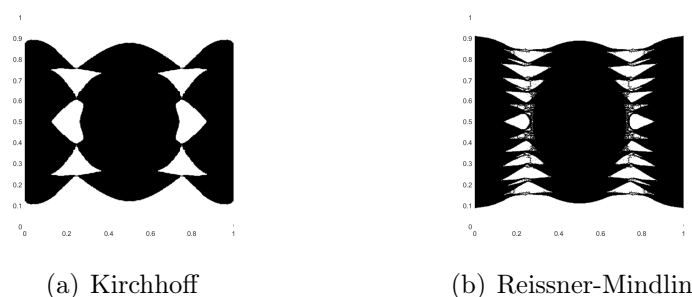## 5.5   Kirchhoff and Reissner-Mindlin Plates: First Eigenvalue Maximization

For the eigenvalue problem we will also consider for both problems (Kirchhoff and Reissner-Mindlin) a hold-all domain Ω given by a clamped square on the left

and right sides and simply supported on the top and bottom sides of dimensions $(0,1) \times (0,1)\mathrm{m}^2$. The non-structural concentrated mass is represented by black dot (see Figure 25). The Young modulus is $E = 210\mathrm{GPa}$, Poisson ratio $\nu = 0.3$ and the plate thickness is $h = 0.05\mathrm{m}$. The contrasts are given by $\gamma_\alpha = \gamma_\rho = 10^{-3}$ and the penalty parameter is set as $\mu = 1.2$. The domain's sensitivity is computed using eq. 56 for Kirchoff plate and eq. 71 for Reissner-Mindlin plate. The experiments are labeled as Cases E1 and E2 for Reissner-Mindlin and Kirchhoff plates, respectively. The final topologies are presented in Fig. 22(a)-(b). Finally, the history of the normalized first eigenvalue λ^1/λ_0^1 (with $\lambda_0^1 = 311.38$ and $\lambda_0^1 = 286.52$ for Kirchhoff and Reissner-Mindlin cases, respectively), volume fraction and shape function obtained during the iterative process are presented in Fig. 23 to Fig. 24. The domain is discretized by using linear triangular finite elements resulting in an initial uniform mesh with $10,000$ elements and $5,101$ nodes. In order to increase the accuracy as well as the topology smoothness 3 steps of uniform mesh refinement during the iterative process are allowed, leading to a mesh with $640,000$ elements and $320,801$ nodes.
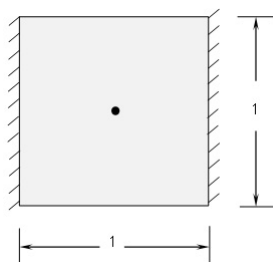
Figure 21: Initial domain for the Kirchhoff and Reissner-Mindlin plates

In Reissner-Mindlin case (Fig. 22(b)) it is observed the presence of small structures due to the numerical artefacts. The mesh refinement isn't enough to overcome this issue even if a higher mesh resolution is imposed. It is well-know that there is a lack of sufficient optimality conditions for such shape optimization problems, so that thin components like those pointed out may appear. In spite of the presence of small structures a local minimum has been reached up to a small numerical tolerance.

(a) Kirchhoff   (b) Reissner-Mindlin

Figure 22: Final Topologies

(a) Kirchhoff   (b) Reissner-Mindlin
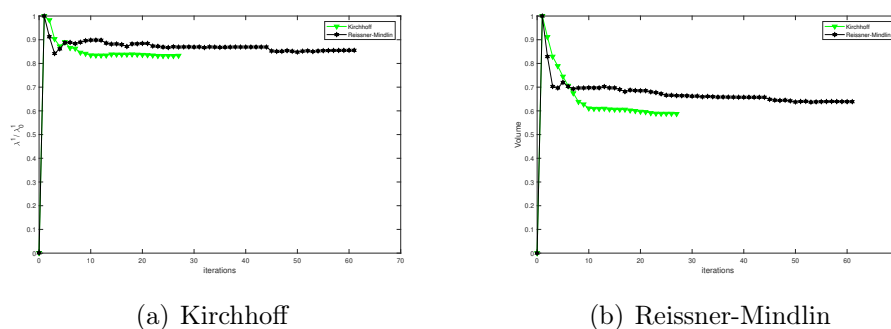
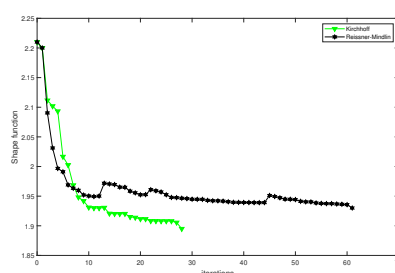**Figure 23: Eigenvalue λ^1/λ_0^1 (a) and Volume Fraction history (b)**

**Figure 24: Shape Function history**

5.6   Compliance Minimization

In the numerical experiment we consider for both problems (Kirchhoff and Reissner-Mindlin) a hold-all domain Ω given by a clamped square of dimensions $(0,1) \times (0,1)\text{m}^2$ submitted to concentrated forces, perpendicular to the plane of the plate, of values $f = -1\text{MN}$ located at the centre of plate. A circular elastic support of radius 0.2m and center at $(0.50, 0.50)$ is also considered (see sketch in Fig. 25(a)-(b). The concentrated loads is represented by black dot whereas the support is represented by a hatched circular area in grey color. The Young modulus is $E = 210\text{GPa}$, Poisson ratio $\nu = 0.3$, the stiffness of the elastic support is $s = 10^{-2}E$ and the plate thickness is $h = 0.05\text{m}$. The contrasts are given by $\gamma_\alpha = \gamma_\rho = 10^{-4}$ and the penalty parameter is set as $\mu = 1.7$. The domain's sensitivity is computed using eq. 73 for Kirchhoff plate and eq. 75 for Reissner-Mindlin plate. The experiments are labeled as Cases C1 and C3 for Reissner-Mindlin with and without support, respectively and Cases C2 and C4 for Kirchhoff with and without support, respectively. The final topologies are presented in Fig. 26(b)-(d) and Fig. 26(a)-(c) for Kirchhoff (Cases C2 and C4) and Reissner-Mindlin (Cases C1 and C3) plates, respectively. Finally, the history of the compliance, volume fraction and shape function obtained during the iterative process are presented in Fig. 27 to Fig. 29.

In addition, the domain is discretized by using linear triangular finite elements resulting in an initial uniform mesh with $14,400$ elements and $7,321$ nodes. In order to increase the accuracy as well as the topology smoothness 3 steps of uniform mesh refinement during the iterative process are allowed, leading to a mesh with $921,600$ elements and $461,761$ nodes.
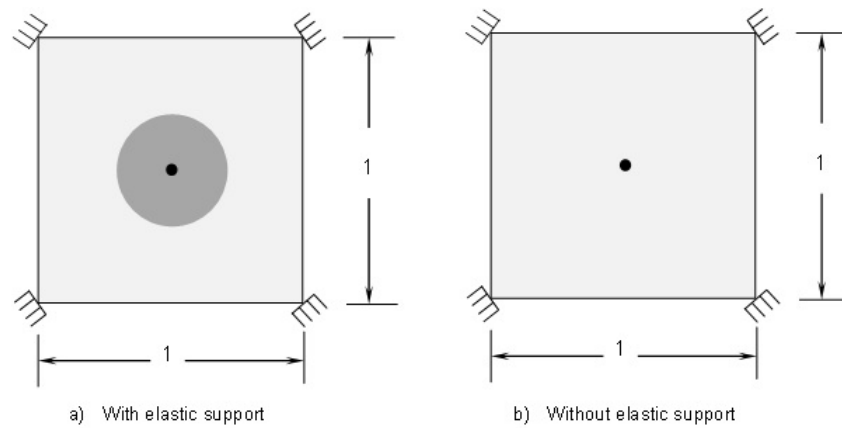
Figure 25: Initial domain with support (a) and without support (b). The concentrated loads are represented by black dots whereas the elastic support is represented by a hatched circular area in grey color

(a) **with support: Case C1**

(b) **with support: Case C2**

(c) **without support: Case C3**

(d) **without support: Case C4**
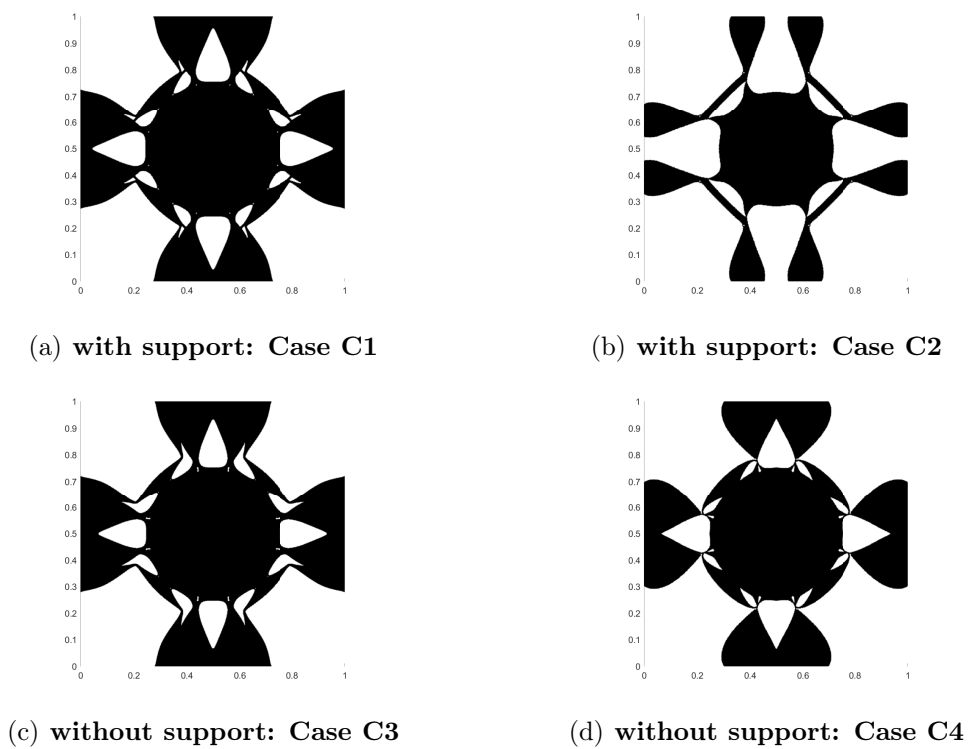
Figure 26: Final Topologies

6   Final remarks

In this chapter the D_T concept was introduced for classic problems of topology optimization. This methodology can be also extended to other applications as inverse problems and image processing. The D_T measures the sensitive of a domain when a singular perturbation is inserted inside the domain. According to this statement it is possible to glimpse that this methodology becomes suitable for detecting the presence of damage in structures. The presence of holes, cracks, or inclusions are
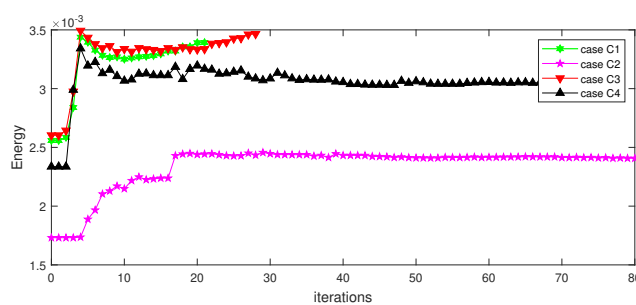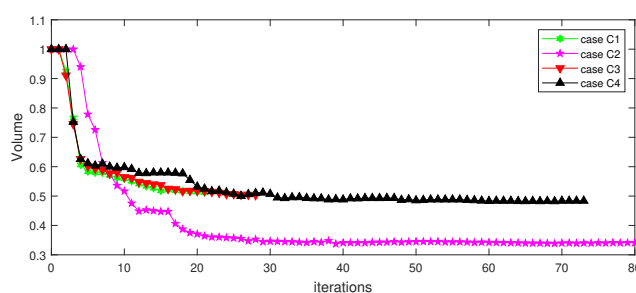
Figure 27: Compliance history

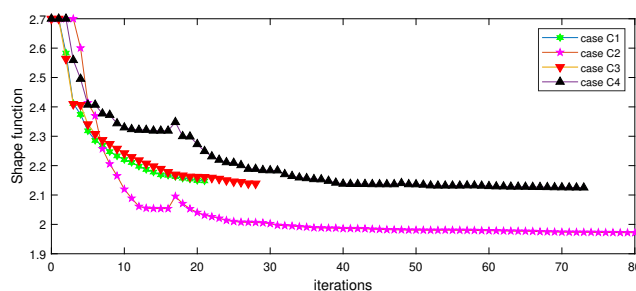**Figure 28: Volume Fraction history**

Figure 29: Shape Function history

typical examples of damages that can be evaluated by employing the appropriate D_T closed formulae to map those problematic regions. Based on this approach, the inverse problem can also be addressed by coupling the appropriate topological derivative to probabilistic optimizations methods. Furthermore, there are no constraint restrictions in the use of the present methodology with numerical methods for the direct problem, such as the finite element method, the boundary element method, or any other numerical method used for the discretization of the quantity of interest in the domain.

7   References

H. Ammari and A. Khelifi. Electromagnetic scattering by small dielectric inhomogeneities. *ournal de Mathématiques Pures et Appliquées*, 82:749–842, 2003.

S. Amstutz and H. Andrä. A new algorithm for topology optimization using a level-set method. *Journal of Computational Physics*, 216(2):573–588, 2006.

S. Amstutz and A. A. Novotny. Topological optimization of structures subject to von mises stress constraints. *Structural and Multidisciplinary Optimization*, 41 (3):407–420, 2010.

S. Amstutz and A. A. Novotny. Topological asymptotic analysis of the Kirchhoff plate bending problem. *ESAIM Control. Optim. Calc. Var.*, 17(3):705–721, 2011. doi: DOI:10.1051/cocv/2010010.

S. Amstutz, I. Horchani, and M. Masmoudi. Crack detection by the topological gradient method. *Control and Cybernetics*, 34(1):81–101, 2005.

C. Anflor, E. Albuquerque, and L. Wrobel. A topological optimization procedure applied to multiple region problems with embedded sources. *International Journal of Heat and Mass Transfer*, 78:121–129, 2014.

C. Anflor, K. Teotônio, and J. Goulart. Structural optimization using the boundary element method and topological derivative applied to a suspension trailing arm. *Engineering Optimization*, 50(10):1662–1680, 2018.

C. T. Anflor and R. J. Marczak. A boundary element approach for topology design in diffusive problems containing heat sources. *International Journal of Heat and Mass Transfer*, 52(19):4604–4611, 2009. ISSN 0017-9310. doi: https://doi.org/10.1016/j.ijheatmasstransfer.2009.02.048. URL `https://www.sciencedirect.com/science/article/pii/S0017931009002580`.

C. T. M. Anflor. *Otimização evolucionária e topológica em problemas governados pela equação de Poisson empregando o método dos elementos de contorno*. PhD Thesis - Federal University of Rio Grande do Sul, 2007.

C. Bertsch, A. P. Cisilino, S. Langer, and S. Reese. Topology Optimization of 3D Elastic Structures Using Boundary Elements. *PAMM*, 8(1):10771–10772, dec 2008. ISSN 16177061. doi: 10.1002/pamm.200810771. URL `http://doi.wiley.com/10.1002/pamm.200810771`.

A. Carpio and M. Rapún. Solving inhomogeneous inverse problems by topological derivative methods. *Inverse Problems*, 24(4):045014, 2008.

F. S. Carvalho. *Análise de sensibilidade topológica aplicada em problemas elípticos*. PhD Thesis - University of Brasilia, 2020.

F. S. Carvalho, D. Ruscheinsky, S. Giusti, C. Anflor, and A. Novotny. Topological derivative-based topology optimization of plate structures under bending effects. *Structural and Multidisciplinary Optimization*, pages 1–14, 2020.

J. Céa, S. Garreau, P. Guillaume, and M. Masmoudi. The shape and topological optimizations connection. *Computer methods in applied mechanics and engineering*, 188(4):713–726, 2000.

L. Comino, R. Gallego, and G. Rus. Combining topological sensitivity and genetic algorithms for identification inverse problems in anisotropic materials. *Computational Mechanics*, 41(2):231–242, 2008.

A. da Silva and A. Novotny. Damage identification in plate structures based on the topological derivative method. *Structural and Multidisciplinary Optimization*, 65 (1):1–12, 2022.

S. Garreau, P. Guillaume, and M. Masmoudi. The topological gradient. Technical report, Université Paul Sabatier - Toulouse 3, France, 1998.

S. Garreau, P. Guillaume, and M. Masmoudi. The topological asymptotic for PDE systems: the elasticity case. *SIAM journal on control and optimization*, 39(6): 1756–1778, 2001.

R. T. Haftka and Z. Gürdal. *Elements of structural optimization*. Kluwer, Dordrecht, third edition, 1992.

M. Hintermüller and A. Laurain. Multiphase image segmentation and modulation recovery based on shape and topological sensitivity. *Journal of Mathematical Imaging and Vision*, 35(1):1–22, 2009.

I. Larrabide, R. Feijóo, A. Novotny, and E. Taroco. Topological derivative: a tool for image processing. *Computers & Structures*, 86(13-14):1386–1403, 2008.

Marczak. Optimization of elastic structures using boundary elements and a topological-shape sensitivity formulation. *Latin American Journal of Solids and Structures*, pages 99–117, 2008.

A. Martinez Dominguez, A. Gümes Gordo, J. M. Perales Perales, and J. Vega de Prada. Topological derivative methods for damage detection. 2018.

S. Nazarov and J. Sokolowski. Shape sensitivity analysis of eigenvalues revisited. *Control and Cybernetics*, 37(4):999–1012, 2008.

A. Novotny, R. Feijóo, E. Taroco, and C. Padra. Topological sensitivity analysis for three-dimensional linear elasticity problem. *Computer Methods in Applied Mechanics and Engineering*, 196(41-44):4354–4364, 2007.

A. A. Novotny and J. Sokolowski. *Topological derivatives in shape optimization. Interaction of Mechanics and Mathematics*. Springer, Berlin, 2013.

A. A. Novotny, R. A. Feijóo, E. Taroco, and C. Padra. Topological sensitivity analysis. *Comput. Methods Appl. Mech. Eng.*, 2003. ISSN 00457825. doi: 10.1016/S0045-7825(02)00599-6.

S. Rocha and A. Novotny. Obstacles reconstruction from partial boundary measurements based on the topological derivative concept. *Structural and Multidisciplinary Optimization*, 55(6):2131–2141, 2017.

D. Ruscheinsky, F. Carvalho, C. Anflor, and A. A. Novotny. Topological asymptotic analysis of a diffusive–convective–reactive problem. *Engineering Computations*, 2020a.

D. Ruscheinsky, F. S. Carvalho, C. Anflor, and A. A. Novotny. Topological asymptotic analysis of a diffusiveâconvectiveâreactive problem. *Engineering Computations*, 2020b.

V. Sales, A. A. Novotny, and J. E. Muñoz Rivera. Energy change to insertion of inclusions associated with the Reissner-Mindlin plate bending model. *Int. J. Solids Struct.*, 59:132–139, may 2015. ISSN 00207683. doi: 10.1016/j.ijsolstr.2015.01.019.

A. Schumacher. Topologieoptimierung von bauteilstrukturen unter verwendung von lochpositionierungskriterien [phd thesis]. *Forschungszentrum für Multidisziplinäre Analysen und Angewandte Strukturoptimierung. Institut für Mechanik und Regelungstechnik*, 1996.

A. P. Seyranian, E. Lund, and N. Olhoff. Multiple eigenvalues in structural optimization problems. *Structural optimization*, 8(4):207–227, 1994.

J. Sokołowski and A. Żochowski. On topological derivative in shape optimization. Technical report, INRIA-Lorraine, France, 1997.

J. Sokolowski and A. Zochowski. Topological derivatives for elliptic problems. *Inverse Probl.*, 15(1):123–134, feb 1999. ISSN 0266-5611. doi: 10.1088/0266-5611/15/1/016. URL http://stacks.iop.org/0266-5611/15/i=1/a=016?key=crossref.f22a4f973d8108972926691f51b74278.

A. J. Torii and J. Rocha de Faria. Structural optimization considering smallest magnitude eigenvalues: a smooth approximation. *Journal of the Brazilian Society of Mechanical Sciences and Engineering*, 39(5):1745–1754, 2017.

Z. Zhang, W. Chen, and X. Cheng. Sensitivity analysis and optimization of eigenmode localization in continuum systems. *Structural and Multidisciplinary Optimization*, 52:305–317, 2015.